The Effect of Ligand Dynamics on Heme Electronic Transition Band III in Myoglobin

Karin Nienhaus,* Don C. Lamb,*† Pengchi Deng,* and G. Ulrich Nienhaus*†

*Department of Biophysics, University of Ulm, 89069 Ulm, Germany and †Department of Physics, University of Illinois at Urbana-Champaign, Urbana, Illinois 61801 USA

ABSTRACT   Band III is a near-infrared electronic transition at $\sim$13,000 cm^{-1} in heme proteins that has been studied extensively as a marker of protein conformational relaxation after photodissociation of the heme-bound ligand. To examine the influence of the heme pocket structure and ligand dynamics on band III, we have studied carbon monoxide recombination in a variety of myoglobin mutants after photolysis at 3 K using Fourier transform infrared temperature-derivative spectroscopy with monitoring in three spectral ranges, (1) band III, the mid-infrared region of (2) the heme-bound CO, and (3) the photodissociated CO. Here we present data on mutant myoglobins V68F and L29W, which both exhibit pronounced ligand movements at low temperature. From spectral and kinetic analyses in the mid-infrared, a small number of photoproduct populations can be distinguished, differing in their distal heme pocket conformations and/or CO locations. We have decomposed band III into its individual photoproduct contributions. Each photoproduct state exhibits a different "kinetic hole-burning" (KHB) effect, a coupling of the activation enthalpy for rebinding to the position of band III. The analysis reveals that the heme pocket structure and the photodissociated CO markedly affect the band III transition. A strong kinetic hole-burning effect results only when the CO ligand resides in the docking site on top of the heme group. Migration of CO away from the heme group leads to an overall blue shift of band III. Consequently, band III can be used as a sensitive tool to study ligand dynamics after photodissociation in heme proteins.

INTRODUCTION

Proteins are complex macromolecules performing a diverse set of functional processes in living systems. A quantitative, predictive understanding of protein function has to be based on both structural and dynamic properties of the protein (Nienhaus and Young, 1996). Detailed investigations of this kind are only feasible for a few well selected model systems. Myoglobin (Mb), a small monomeric heme protein of $\sim$18 kD, is an excellent choice for this endeavor. Its polypeptide chain consists of 153 amino acids that are folded into eight α-helices. These are wrapped around a heme prosthetic group, which is covalently linked through its central Fe^{2+} ion to the proximal histidine (H93) (Antonini and Brunori, 1971; Dickerson and Geis, 1983; Stryer, 1995). Small ligands such as O$_2$, NO, or CO bind reversibly to the heme iron from an internal cavity, the distal heme pocket. A large number of experimental and theoretical studies as well as computer simulations have revealed an enormous complexity in the apparently simple biological process of ligand binding (Austin et al., 1975; Elber and Karplus, 1990).

Flash photolysis experiments performed on carbonmonoxymyoglobin (MbCO) and oxymyoglobin (MbO$_2$) over wide ranges of time and temperature have shown that ligand binding involves multiple intermediate states (Austin et al.,

1975). In recent years cryocrystallography experiments of photolyzed MbCO (Schlichting et al., 1994; Teng et al., 1994; Hartmann et al., 1996; Brunori et al., 2000; Ostermann et al., 2000; Chu et al., 2000) have shown that these intermediates arise from transient binding sites of ligands in internal protein cavities, the "xenon" holes (Tilton et al., 1984). From these studies, a picture has emerged for CO binding under physiological conditions in which the ligand, after entering the protein from the solvent, shuttles back and forth many times among the various cavities. The probability that the ligand binds to the heme iron is small, typically only a few percentage points. In most instances, the CO returns to the solvent without binding.

Knowledge of the intermediate states is a prerequisite for understanding the dynamic aspects of the binding reaction, i.e., the temporal sequence of ligand transitions among the various sites as well as the accompanying protein fluctuations and relaxations. These processes can be investigated through measurements of spectral shifts in the electronic absorption bands of the heme group (Šrajer and Champion, 1988; Steinbach et al., 1991; Ahmed et al., 1991; Lambright et al., 1991; Ansari et al., 1992; Nienhaus et al., 1992; Lim et al., 1993; Huang et al., 1997; Stavrov, 2001). In these studies, the near-infrared band III, an $a_{2u}(\pi) \rightarrow d_{yz}$ charge-transfer transition at $\sim$760 nm ($\sim$13 000 cm^{-1}) that appears only in the deligated, five-coordinate form, has played a key role (Iizuka et al., 1974; Eaton and Hofrichter, 1981; Sassaroli and Rousseau, 1987; Cordone et al., 1990; Chavez et al., 1990; Xie and Simon, 1991; Šrajer and Champion, 1991; Jackson et al., 1994). Its sensitivity to protein structure is most dramatically seen in the so-called kinetic hole-burning (KHB) effect that is observed at temperatures be-

low ~180 K (Agmon, 1988; Campbell et al., 1987; Steinbach et al., 1991): In this temperature region, proteins are frozen into different conformational substates with slightly different molecular structures and barriers for ligand binding. Consequently, band III decays in a nonexponential fashion as ligands rebind. Moreover, an apparent spectral shift is observed that arises from a correlation between the peak frequency of the spectral band and the barrier for recombination. Upon photolysis at room temperature, band III also shifts over many orders of magnitude in time, from picoseconds to microseconds. Anfinrud and coworkers attributed the shift to the temporal evolution of the iron-heme displacement (Lim et al., 1993, 1997; Jackson et al., 1994). However, from the x-ray structures of photoproducts it has become apparent that most of the displacement of the iron upon ligand dissociation is elastic and occurs even in a frozen protein at 20–40 K (Schlichting et al., 1994; Teng et al., 1994; Hartmann et al., 1996). Results from Stark-effect spectroscopy suggest, however, that the electrostatic environment of the heme pocket influences the properties of heme transitions (Franzen et al., 1999). The specific structural changes responsible for the observed shifts have remained obscure as of yet.

To elucidate the sensitivity of band III to the distal heme pocket structure, we have studied photolysis-induced ligand dynamics in a number of MbCO mutants at low temperatures using three different spectroscopic markers, (1) the electronic transition band III in the near-infrared (NIR) and the stretch absorption of (2) the heme-bound CO as well as (3) the photodissociated CO in the mid-infrared (MIR). From spectroscopic and kinetic information in the MIR region, we can distinguish between different distal heme pocket structures and observe migration of CO among different sites in the heme pocket. We quantitatively decompose band III into contributions of the various photoproduct states, taking V68F and L29W MbCO as examples. The analysis reveals a substantial influence of heme pocket structural changes, most importantly ligand movements, on band III.

Bound and photoproduct states in L29W MbCO

Proteins can assume a large number of conformational substates, represented by local minima in a complex conformational energy landscape. In the energy landscape of MbCO, a small number of taxonomic substates (also denoted as A substates) can be distinguished, each of which comprises a large number of statistical substates (Frauenfelder et al., 1991). The taxonomic substates are characterized by different IR stretch bands of the heme-bound CO near 5 μm. Interaction of the CO dipole with the local electric field (Stark effect) in the distal heme pocket is the major determinant generating multiple CO stretch bands (Oldfield et al., 1991; Kushkuley and Stavrov, 1996), as shown experimentally by studies of many distal pocket
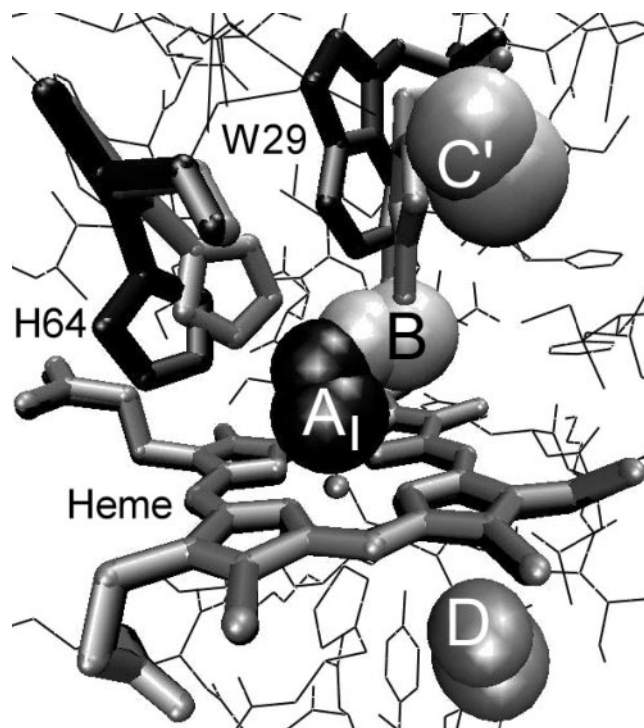

FIGURE 1 Model of the L29W mutant MbCO (A_I substate) from the x-ray structure analysis at 105 K, showing the heme group and the side chains of H64 and W29. Also included are the CO positions in the B, C', and D photoproduct states.

mutants of myoglobin (Braunstein et al., 1993; Li et al., 1994; Phillips et al., 1999).

L29W MbCO is a particularly interesting mutant that we have characterized both structurally and spectroscopically (Ostermann et al., 2000). It exhibits two taxonomic substates, A_I and A_{II} (at pH ~7), which are associated with CO bands at ~1945 cm^{-1} and ~1958 cm^{-1}, respectively. Below the dynamical transition temperature at ~180 K (Nienhaus et al., 1989; Kneller and Smith, 1994; Ostermann et al., 2000), each molecule is frozen into one or the other A substate, and thus, their relative populations are fixed, with A_I as the dominant species. Above ~180 K, A_{II} grows at the expense of A_I, and by 300 K, essentially the entire population has shifted to the A_{II} substate.

Fig. 1 shows essential features of the L29W MbCO crystal structure at 105 K, including the heme group and the side chains of H64 and W29, as well as the CO ligand in the bound and the various photoproduct states (Ostermann et al., 2000). The bound ligand is labeled A_I. For this conformation, the side chains of the distal histidine (H64) and tryptophan B10 (W29) are depicted in dark gray. Also shown are the CO locations in the photoproduct states $B(A_I)$ on top of heme pyrol C and $C'(A_I)$ in the xenon 4 cavity. Both these photoproduct states can be populated upon photolysis below ~180 K, and except for the movement of the iron by 0.3 Å out of the heme plane, no other significant

structural changes occur. After photodissociation above $\sim$180 K, the ligand is found in state D on the proximal side, and the side chains of H64 and W29 rearrange markedly (light gray) so that the W29 indole ring adopts the same conformation as in the room temperature bound-state structure (Hirota et al., 1996). It is reasonable to assume that this conformation is also characteristic of the A_{II} minority species at low temperature. In this conformation, the indole ring not only interferes with ligand binding in the docking site on the heme, it also prevents access of the ligand to the xenon 4 cavity.

MATERIALS AND METHODS

Sample preparation

Sperm whale myoglobin mutants L29W and V68F were expressed in *Escherichia coli*, purified as described previously (Springer et al., 1989) and stored in lyophilized form. For the experiments, the protein powder was dissolved at a concentration of $\sim$15 mM in cryosolvent (75% glycerol/25% potassium phosphate buffer (v/v), pH 7.5), stirred under a CO atmosphere, and reduced with sodium dithionite solution. A few microliters of the sample solution were sandwiched between two CaF$_2$ windows (diameter 25.4 mm) separated by a 130-μm thick mylar washer.

Fourier transform IR (FTIR)-cryospectroscopy

The windows were kept inside a block of oxygen-free high-conductivity copper mounted on the cold-finger of a closed-cycle helium refrigerator (model SRDK-205AW, Sumitomo, Tokyo, Japan), which allowed us to adjust the sample temperature in the range between 3 and 320 K. The temperature was measured with a silicon temperature sensor diode and regulated with a digital temperature controller (model 330, Lake Shore Cryotronics, Westerville, OH). Samples were photolyzed with a continuous wave, frequency doubled Nd-YAG laser (model Forte 530–300, Laser Quantum, Manchester, UK), operated at 300 mW output at 532 nm. The laser beam was split and focused on the sample from both sides. Transmission spectra were collected in the NIR between 12 000 and 14 000 cm^{-1} with a resolution of 8 cm^{-1}, and in the MIR between 1800 and 2400 cm^{-1} with a resolution of 2 cm^{-1}, using a FTIR spectrometer (IFS 66v/S, Bruker, Karlsruhe, Germany).

Temperature-derivative spectroscopy (TDS)

To assess the rebinding properties of different photoproduct species in the low-temperature experiments, TDS was used, which is an experimental protocol designed to measure thermally activated rate processes with distributed barriers. The method has been described earlier in detail (Berendzen and Braunstein, 1990; Mourant et al., 1993; Nienhaus et al., 1994), and we therefore give only a brief summary here. The TDS measurement is started at the lowest temperature desired after preparation of the sample by illumination. Subsequently, while increasing the sample temperature T linearly in time, FTIR spectra are taken continuously. Difference spectra, $\Delta A(\nu, T)$, are calculated from absorbance spectra, $A(\nu, T)$, at successive temperatures,

$$\Delta A(\nu, T) = A(\nu, T - \tfrac{1}{2} \text{ K}) - A(\nu, T + \tfrac{1}{2} K). \quad (1)$$

For a particular band, the change in spectral area $\Delta(\nu, T)$ that occurs during acquisition of two successive spectra is proportional to the change in the population, ΔN, contributing to the band. In this work, absorption changes arise from ligand rebinding and ligand diffusion among different docking

sites. Both of these processes are governed by thermal activation over enthalpy barriers. The temperature ramp protocol ensures that rebinding occurs sequentially with respect to the height of the activation enthalpy barrier. The barrier height is approximately proportional to the ramp temperature so that the temperature axis can be recast into an enthalpy axis. TDS data are conveniently displayed as contour plots of the absorbance change on a surface spanned by the wave number and temperature axes.

Data analysis

At each temperature, FTIR-TDS transmittance spectra taken after photolysis at 3 K were referenced against transmittance spectra taken in the dark to cancel effects arising from the intrinsic temperature dependence of the spectra. The obtained absorbance spectra were subsequently baseline-corrected. Band III areas were calculated from the absorbance, $\epsilon(\nu)$, as zeroth moments, $M_0 = \int \epsilon(\nu) d\nu$, and band positions were computed as first moments, $M_1 = \int \epsilon(\nu) \nu d\nu / M_0$. For decomposition of the MIR difference spectra of the bound and photodissociated CO into substate populations, the spectra were fitted with gaussian band shapes at each individual temperature. The spectral areas of the gaussians were used to determine the fraction of molecules within a particular photoproduct state.

For V68F MbCO, three nicely resolved photoproduct species are observed in the TDS map of the photolyzed CO into which band III was decomposed in a two-step procedure. In the first step, scale factors were determined that relate the absorbance changes observed upon rebinding in the IR bands of the bound CO (A states) to those observed in the bands of the photodissociated CO (B states). This was done by fitting the temperature dependence of the absorbance integrated over the entire A substate TDS map with a superposition of B substate contributions, as determined from the integrated absorbances in the individual B substate bands. In the second step, an overall scale factor was introduced by which to multiply the temperature dependence of the integrated A substate absorbance to match that of band III.

For L29W MbCO, band III was decomposed on the basis of different A substate populations, and only a single overall factor was necessary for scaling of the TDS data in the MIR and NIR spectral regions.

After the contribution, $C_i(T)$, of each photoproduct state i to rebinding at each temperature was determined from the MIR data, the temperature dependence of M_1 in band III was fitted by a superposition of photoproduct contributions

$$M_1(T) = \sum_i C_i(T) M_{1i} = \sum_i C_i(T)[m_i T + \nu_{0i}], \quad (2)$$

where m_i and ν_{0i} are the slope and offset parameters of the (assumed) linear temperature dependence of band III within the individual photoproduct states.

RESULTS AND DISCUSSION

Ligand dynamics in V68F MbCO

TDS spectra were acquired after photolysis illumination for 1 s at 3 K. The data are shown in Fig. 2 in the NIR band III (panel *a*), the MIR region of the heme-bound CO (panel *b*), and the photodissociated CO (panel *c*). Because band III decays upon rebinding, its TDS map displays mainly negative contours.

Absorption changes are observed over a wide temperature range, indicating that ligand rebinding is governed by a distribution of enthalpy barriers. Around 18 K, positive contours are visible on the red side of the band (Fig. 2 *a*), representing a gain in absorbance. This peculiar behavior
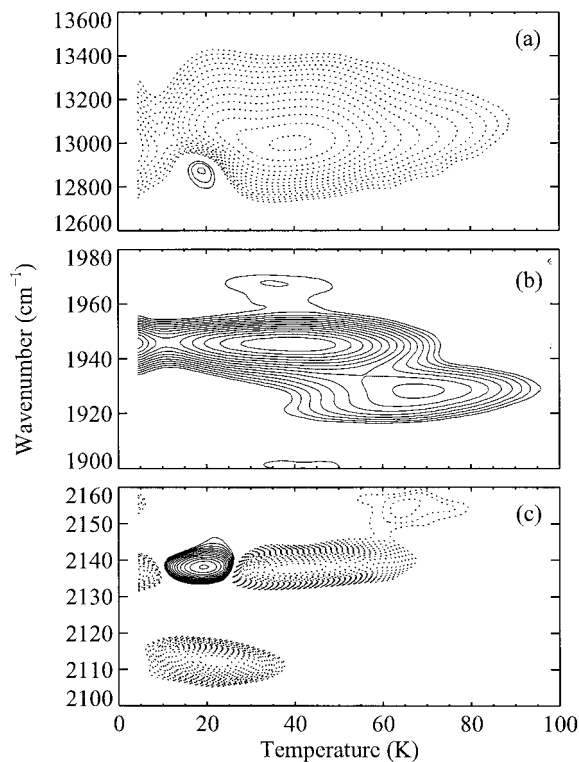
FIGURE 2 TDS maps of V68F MbCO after 1 s photolysis at 3 K; (*a*) NIR band III, (*b*) MIR stretch bands of the heme-bound CO, and (*c*) of the photodissociated CO in the protein. Contours are spaced logarithmically, solid (dashed) lines representing absorbance increase (decrease).

FIGURE 3 (*a*) Decay of band III from the TDS experiment (*symbols*) and decomposition into the three photoproduct contributions based on the *A* and *B* state TDS data in Fig. 2, *b* and *c* (*solid line*: sum of photoproducts). (*b*) Band position M_1 of the spectral change with temperature (symbols) and population-weighted superposition of the three photoproduct contributions (*solid line*).

can be understood from the MIR data taken under identical conditions.

The TDS map in Fig. 2 *b* depicts spectral changes in the IR bands of the heme-bound CO because of rebinding. It looks similar to a TDS map of native MbCO (Mourant et al., 1993), and we can distinguish three taxonomic substates, a barely detectable A_0 at 1966 cm^{-1}, a dominant A_1 at 1945 cm^{-1} with maximum rebinding at 40 K, and an A_3 substate at 1928 cm^{-1} with maximum rebinding at 68 K. Apparently, the barriers to rebinding and the electrostatic environment of the CO in the bound state of V68F MbCO are similar to those in the native protein, despite the introduction of the bulky phenyl ring in the distal heme pocket. This observation is in agreement with the x-ray structure by Quillin et al. (1995), which shows the F68 side chain lining the distal heme pocket wall instead of protruding toward the active site. In the TDS map in the region of the photodissociated CO (panel *c*), there are negative as well as positive contours. The latter represent an increase in the population, which arises from ligand movements. The $B_2(A_1)$ band at 2112 cm^{-1} decays, with maximal loss of population at 18 K, because of both rebinding and population transfer to the $B_1(A_1)$ band at 2138 cm^{-1}. $B(A_3)$ at 2155 cm^{-1} solely rebinds to A_3. Photoproduct x-ray structures are not yet available for the V68F mutant, and thus a definite structural
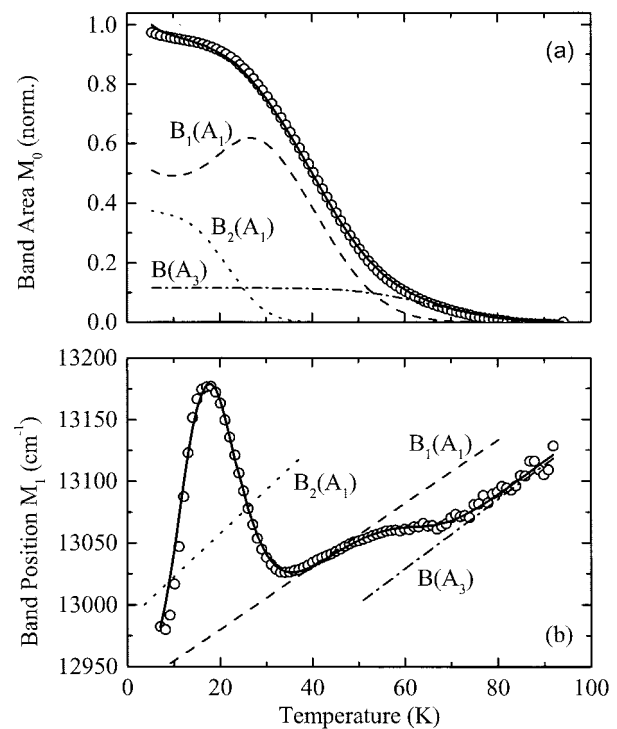
assignment of the three photoproduct states is not yet possible. Molecular dynamics simulations on V68F MbCO (for the predominant A_1 state), however, reveal only a single location of the photolyzed CO (Quillin et al., 1995). Following the interpretation of Anfinrud and coworkers (Lim et al., 1997) for the *B* states at 2119 and 2131 cm^{-1} in native MbCO, which show a similar behavior at ~20 K (Alben et al., 1982), the exchange in Fig. 2 *c* reflects a rotation of CO in the docking site on top of the heme group.

A quantitative analysis of the TDS data enabled us to decompose band III into contributions from its three photoproduct states. From the *A* substate TDS map, Fig. 2 *b*, the fractions of A_0, A_1, and A_3 that rebind at each temperature were determined. The almost negligible population of A_0 was included in A_1 and not treated separately. From the *B* substate map, the individual populations of the three photoproduct states were calculated as a function of temperature. Different overall scale factors (29 for A_1/B_1, 25 for A_1/B_2, and 34 for $A_3/B(A_3)$) were obtained for the *A/B* absorbance ratios in each photoproduct state. The ratio between the integrated absorbances in the *A* bands and in band III was determined as 0.263 ± 0.005. In Fig. 3 *a*, we plot the relative populations of the three photoproduct states as a function of temperature. Their sum agrees well with the

TABLE 1 Parameters of the photoproduct states of MbCO mutants V68F and L29W characterizing KHB in band III

Sample	State	Offset ν_0 [cm^{-1}]	Slope m [cm^{-1}/K]
V68F	$B_1(A_1)$	12937 ± 6	2.5 ± 0.2
	$B_2(A_1)$	13002 ± 10	3.5 ± 0.5
	$B(A_3)$	12872 ± 7	2.8 ± 0.2
L29W	$B^*(A_I/A_{II})$	12991 ± 7	3.0 ± 0.5
	$B(A_I)$	12934 ± 7	2.9 ± 0.2
	$C'(A_I)$	13028 ± 3	0.7 ± 0.2
	$B(A_{II})$	13094 ± 10	0.2 ± 0.2

FIGURE 4 TDS maps of L29W MbCO after 15 000 s photolysis at 3 K; (*a*) NIR band III, (*b*) MIR stretch bands of the heme-bound CO, and (*c*) the photodissociated CO in the distal heme pocket. Contours are spaced logarithmically, solid (dashed) lines representing absorbance increase (decrease).

decay of the photolyzed population as observed in band III. $B_2(A_1)$ starts at 38% and decays at ~20 K by transferring 13% into $B_1(A_1)$; 25% rebind directly once sufficient thermal energy is available for the ligand to overcome the binding energy at the site. $B_1(A_1)$ and $B(A_3)$ decay at ~40 and 70 K, respectively.

In Fig. 3 *b*, the first moments of the TDS spectra of band III are shown as a function of temperature. Note that these are differential data, representing band positions of the spectral change from one temperature to the next. Most notably, the peculiar behavior of band III in Fig. 2 *a* around 18 K appears here as an enormous excursion of the first moment to the blue.

To model the data, we assume that KHB for each photoproduct species obeys a linear dependence of M_1 on temperature (and hence activation enthalpy for rebinding), with offset ν (T = 0) = ν_0 and slope m. The parameters characterizing KHB in each photoproduct were obtained by a fit of the overall first moment, calculated as the population-weighted average of the three photoproduct states, to the data. The solid line through the datapoints represents the overall M_1, the fit parameters are compiled in Table 1. Below ~40 K, rebinding occurs exclusively from $B_1(A_1)$ and $B_2(A_1)$. Their associated band III spectra are markedly different, separated by ~80 cm^{-1} at 20 K, with slopes of 3.5 and 2.5 cm^{-1}/K, respectively. Above ~40 K, the contribution from $B(A_3)$ rebinding comes into play, seen as a transition of M_1 to a third line below that of $B_1(A_1)$, with a slope of 2.8 cm^{-1}/K. We also mention that simulations of the entire band III TDS map with three temperature-invariant, asymmetric band III lines (sum of two gaussians), one for each photoproduct state, with linear KHB dependence on temperature, yielded results identical with the first moment analysis in Fig. 3 *b*.

The excellent agreement between measured spectra (first moments) and calculated superpositions from the three photoproduct states justifies *a posteriori* the assumption of a linear dependence of the wave number on the TDS temperature (and thus the enthalpy barrier for rebinding). The sensitivity of band III to the distal pocket environment is evident from the analysis. Below ~180 K, protein motions are frozen in, so that for $B_2(A_1)$ and $B_1(A_1)$ the pronounced
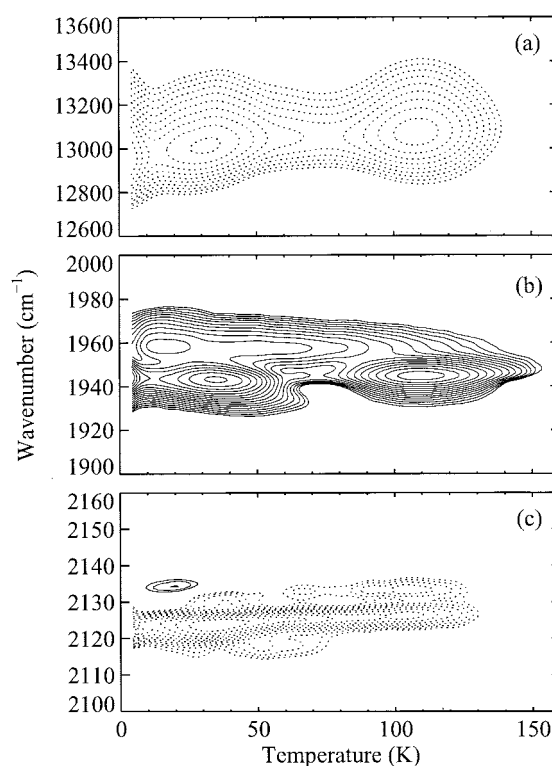
differences in their band III properties arise solely from different ligand conformations in an otherwise unaltered distal heme pocket. For $B(A_3)$, its different distal heme pocket structure, its concomitantly modified CO docking site or both may cause the observed shift to the red by ~50 cm^{-1} with respect to $B_1(A_1)$.

Ligand dynamics in L29W MbCO

To study the influence of ligand migration to another cavity on band III, we chose L29W MbCO, where the photoproduct structures have been determined (Ostermann et al., 2000). Using the same illumination protocol as with V68F (1 s at 3 K), only a tiny fraction of ligands is found in the $C'(A_I)$ site (Fig. 1). To enhance this population, we exposed the sample to the photolysis beam for 15 000 s at 3 K, which ensures that ~50% of the CO molecules migrate from the $B(A_I)$ site on top of the heme group to the $C'(A_I)$ (xenon 4) site in the back of the distal heme pocket. For both short and long illumination, the analysis yields identical properties of the photoproduct states within the experimental error.

In Fig. 4 *b*, the two taxonomic substates, A_I (1945 cm^{-1}) and A_{II} (1958 cm^{-1}), are spectrally resolved. In the dominant species, A_I, the two photoproduct states $B(A_I)$ and
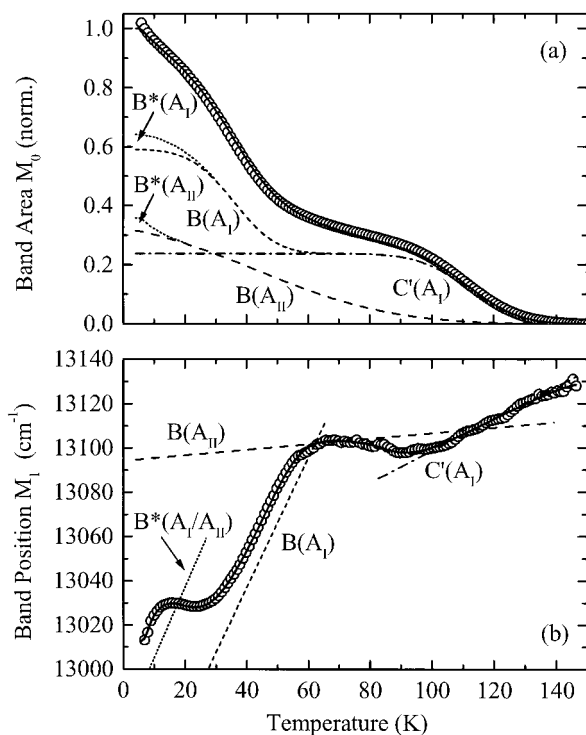
FIGURE 5 (*a*) Decay of band III from the TDS experiment (*symbols*) and decomposition into five photoproduct contributions on the basis of the TDS map in Fig. 4 *b* (*solid line* through the symbols: sum of photoproducts); (*b*) Band position M_1 of the spectral change with temperature (symbols) and population-weighted superposition of the three photoproduct contributions (*solid line*).

$C'(A_I)$ appear in the NIR TDS map in Fig. 4 *a* as peaks of maximal rebinding at 35 and 110 K. For the minority conformation A_{II}, access to the C' site is apparently blocked by the W29 indole side chain (Fig. 1). Rebinding in A_{II} is broadly distributed from the lowest temperatures up to ~140 K, suggesting that it does not occur from a single, well defined CO location. In contrast to the V68F mutant with its three photoproduct species widely separated in the spectral region of the photodissociated CO, Fig. 4 *c* shows little spectral dispersion among the various photoproduct states. Here we only remark that CO residing in the $C'(A_I)$ photoproduct exhibits two clearly separated bands that we associate with two different orientations of the CO molecule. The positive contours below ~30 K are attributable to reorientation of a small fraction of CO molecules within the $C'(A_I)$ (xenon 4) cavity. Because of the poor spectral separation of the photoproduct spectra in Fig. 2 *c*, we performed the decomposition of band III on the basis of the *A* substate TDS data. The scale factor between the integrated absorbances in the *A* bands and in band III was determined as 0.363 ± 0.005.

In Fig. 5 *a*, the decay of band III with temperature is plotted together with the relative fractions of the photoproduct contributions that can be distinguished from the analysis

of the TDS map in Fig. 4 *b*. For A_I, rebinding to the photoproduct species $B(A_I)$ and $C'(A_I)$ is seen as two large steps. A third fraction, $B*(A_I)$, accounts for part of the population below 30 K (Fig. 4 *b*). Similarly, for the minority species, A_{II}, a tiny fraction, denoted with $B*(A_{II})$, seen as a peak near 20 K in Fig. 4 *b* on top of the broad distribution, was treated separately from the main photoproduct species, $B(A_{II})$.

In Fig. 5 *b*, we plot the first moments of the band III TDS spectra as a function of temperature. The solid line results from fitting the data with a superposition of photoproduct states, assuming again linear dependencies between band positions M_1 and temperature. The fit parameters are included in Table 1. In the temperature range below 30 K, $B*(A_I)$ and $B*(A_{II})$ govern the M_1 curve despite their small populations. Within the error, their KHB properties are identical, and thus we have combined them in the analysis. Above 30 K, only $B(A_I)$, $C'(A_I)$, and $B(A_{II})$ contribute to the band III signal. Fortunately, $B(A_{II})$ dominates the recombination signal between 60 and 80 K, which helps to reliably determine the band III parameters. A model calculation of the TDS map of band III was also performed on the L29W data; it gave essentially the same results as fitting first moments.

The photoproduct species $B*(A_I)$, $B*(A_{II})$, and $B(A_I)$ are characterized by steep KHB dependencies, with identical slopes within the error of the data (3 and 2.9 cm^{-1}/K). By contrast, the slopes of both $B(A_{II})$ and $C'(A_I)$ are much smaller, (0.2 and 0.7 cm^{-1}/K, respectively), and both photoproducts contribute further to the blue (~13 100 cm^{-1}). We conclude that migration of the CO away from the docking site at the heme iron leads to a blue shift and a substantially weakened KHB. The x-ray structure analysis shows that ligand migration at low temperature happens in the absence of structural changes in the protein moiety (Ostermann et al., 2000). Therefore, the interaction of the heme group with the CO molecule itself must be responsible for the strong KHB effect in band III.

The residual slope of 0.7 cm^{-1}/K deserves a remark. According to our kinetic data, recombination from $C'(A_I)$ involves crossing two enthalpy barriers in succession, first $H_{C'B}$, then H_{BA}, the first one being rate-limiting. Thus, the broad barrier distribution reflected in the width of the peak at 110 K (Fig. 4 *b*) is caused by structural heterogeneity in the channel between the $B(A_I)$ and $C'(A_I)$ sites. The amino acids involved, such as W29, I107, and H64, evidently have an effect on the band III position, although much weaker than the effect of the CO ligand itself.

For lack of an x-ray structure of $B(A_{II})$, we can merely speculate about its structural properties. The weak KHB effect suggests that the ligand is not in direct contact with the heme group.

CONCLUSIONS

In this work, we have decomposed the electronic transition band III into its contributions from different photoproduct species within each bound-state conformation (*A* substate) on the basis of their spectroscopic differences and ligand-binding properties. It has become evident that band III is exquisitely sensitive to structural details in the distal heme pocket, most importantly, the presence or absence of the CO near the heme after dissociation from the central iron. Fig. 5 *b* shows that band III shifts to the blue by $\sim$60 cm^{-1} when the CO diffuses away from the docking site *B* on top of pyrrol *C*. This shift was observed earlier in wild type MbCO (Nienhaus et al., 1992), but could not at that time be attributed to ligand migration because of lack of structural information. Rather, the focus of that paper was on a second blue shift of band III by $\sim$60 cm^{-1} at the dynamical transition temperature at $\sim$180 K, which also occurs in the mutants studied here (data not shown). This second shift was taken as evidence of large-scale conformational changes around the heme group, and the work on L29W by Ostermann et al. (2000) has indeed shown that conformational fluctuations are sufficiently large above 180 K to open channels for the CO to migrate into cavity *D* on the proximal side (Fig. 1).

Anfinrud and coworkers measured the shift of band III in photolyzed MbCO at room temperature over the enormous time range from 2 ps to 56 μs (Lim et al., 1993; Jackson et al., 1994). The time dependence of the band III shift by $\sim$120 cm^{-1} was shown to be strongly nonexponential and modeled with a stretched exponential, $\exp[-kt]^{\beta}$, with stretching exponents β in the range of 0.03–0.18, depending on the fit procedure. Such small stretching exponents suggest that multiple processes occurring in succession are responsible for the band shift, and not a single process. Closer inspection of the data reveals a distinct rapid shift by $\sim$60 cm^{-1} up to $\sim$20 ps, followed by a slow shift of similar amplitude extending into the microsecond time scale. Because of the charge-transfer character of band III, the observed band shifts had previously been solely attributed to protein relaxation on the proximal side of the heme, caused by movement of the iron out of the heme plane after ligand dissociation (Šrajer and Champion, 1991; Nienhaus et al., 1992; Lim et al., 1993). The sensitivity of the intensity, position, and width of band III to the extent of iron-heme displacement was recently analyzed in a theoretical paper by Stavrov (2001). There it was concluded that the intensity of band III should be used as a marker for the iron displacement, and not the position or the width, as the latter two may also be affected by other factors. Our present work proves that structural changes on the distal side, in particular ligand migration, contribute significantly to the shift of band III.

This raises the question as to how to separate the blue shift of band III at room temperature into the two effects, iron-out of plane relaxation, and structural changes in the environment of the chromophore. Most of the iron displacement is expected to be very fast at room temperature, because $\sim$80% of the shift happens even in a frozen protein (Schlichting et al., 1994; Teng et al., 1994; Hartmann et al., 1996; Brunori et al., 2000; Ostermann et al., 2000; Chu et al., 2000) and thus does not involve slow, collective protein motions. Huang et al. (1997) observed KHB in band III on the nanosecond time scale at 293 K when they embedded the proteins in highly viscous solvents, which suggests that part of the proximal relaxation is governed by collective protein modes that are coupled to the dynamics of the solvent environment. Following the argumentation by Stavrov (2001), the iron dynamics may be directly observed by measuring the time evolution of the band III absorbance. Lim et al. (1993) have presented band III spectra of photo-dissociated MbCO at 1.78, 17.8, 178, and 1780 ps and stated that the integrated area doubles from 1.78 ps to 17.8 ps and is constant thereafter. This observation supports our view that the first phase of the band III shift at room temperature by 60 cm^{-1}, which extends out to $\sim$20 ps (Jackson et al., 1994), should be attributed mainly to the iron out-of-plane relaxation.

The second, slower phase of band III shift covers several orders of magnitude in time, from $\sim$20 ps to microseconds. Such a wide spectrum of characteristic times is typical of large-scale protein rearrangements in response to structural changes at the active site (Johnson et al., 1996; Nienhaus and Young, 1996; McMahon et al., 1998; Engler et al., 2000). Whereas ligand diffusion within the heme pocket has been suggested to occur on the picosecond time scale by molecular dynamics simulations (Elber and Karplus, 1990; Brunori et al., 1999) or NO rebinding experiments at room temperature (Olson and Phillips, 1996), ligand migration to other internal cavities or to the solvent is expected to occur on longer time scales because it is controlled by protein fluctuations that transiently open passageways. We thus attribute the slower phase of the band III shift to ligand migration and structural relaxations around the heme group. The sensitivity of this electronic transition to the iron displacement from the heme plane *and* the heme structural environment makes it a superb tool in the study of structure-dynamics-function relations in heme proteins.

REFERENCES

Agmon, N. 1988. Reactive line-shape narrowing in low-temperature inhomogeneous geminate recombination of CO to myoglobin. *Biochemistry.* 27:3507–3511.

Ahmed, A. M., B. F. Campbell, D. Caruso, M. R. Chance, M. D. Chavez, S. H. Courtney, J. M. Friedman, I. E. Iben, M. R. Ondrias, and M. Yang.

1991. Evidence for proximal control of ligand specificity in hemeproteins: absorption and Raman studies of cryogenically trapped photoproducts of ligand bound myoglobins. *Chem. Phys.* 158:329–352.

Alben, J. O., D. Beece, S. F. Bowne, W. Doster, L. Eisenstein, H. Frauenfelder, D. Good, J. D. McDonald, M. C. Marden, P. P. Moh, L. Reinisch, A. H. Reynolds, E. Shyamsunder, and K. T. Yue. 1982. Infrared spectroscopy of photodissociated carboxymyoglobin at low temperatures. *Proc. Natl. Acad. Sci. U.S.A.* 79:3744–3748.

Ansari, A., C. M. Jones, E. R. Henry, J. Hofrichter, and W. A. Eaton. 1992. The role of solvent viscosity in the dynamics of protein conformational changes. *Science.* 256:1796–1798.

Antonini, E., and M. Brunori. 1971. Hemoglobin and Myoglobin in their Reactions with Ligands. North-Holland, Amsterdam.

Austin, R. H., K. W. Beeson, L. Eisenstein, H. Frauenfelder, and I. C. Gunsalus. 1975. Dynamics of ligand binding to myoglobin. *Biochemistry.* 14:5355–5373.

Berendzen, J., and D. Braunstein. 1990. Temperature-derivative spectroscopy: a tool for protein dynamics. *Proc. Natl. Acad. Sci. U.S.A.* 87:1–5.

Braunstein, D. P., K. Chu, K. D. Egeberg, H. Frauenfelder, J. R. Mourant, G. U. Nienhaus, P. Ormos, S. G. Sligar, B. A. Springer, and R. D. Young. 1993. Ligand binding to heme proteins: III. FTIR studies of His-E7 and Val-E11 mutants of carbonmonoxymyoglobin. *Biophys. J.* 65:2447–2454.

Brunori, M., F. Cutruzzolà, C. Savino, C. Travaglini-Allocatelli, B. Vallone, and Q. H. Gibson. 1999. Structural dynamics of ligand diffusion in the protein matrix: a study on a new myoglobin mutant Y(B10) Q(E7) R(E10). *Biophys. J.* 76:1259–1269.

Brunori, M., B. Vallone, F. Cutruzzolà, C. Travaglini-Allocatelli, J. Berendzen, K. Chu, R. M. Sweet, and I. Schlichting. 2000. The role of cavities in protein dynamics: crystal structure of a photolytic intermediate of a mutant myoglobin. *Proc. Natl. Acad. Sci. U.S.A.* 97:2058–2063.

Campbell, B. F., M. R. Chance, and J. M. Friedman. 1987. Linkage of functional and structural heterogeneity in proteins: dynamic hole burning in carboxymyoglobin. *Science.* 238:373–376.

Chavez, M. D., S. H. Courtney, M. R. Chance, D. Kiula, H. Nocek, B. M. Hoffman, J. M. Friedman, and M. R. Ondrias. 1990. Structural and functional significance of inhomogeneous line broadening of band III in hemoglobin and Fe-Mn hybrid hemoglobins. *Biochemistry.* 29:4844–4852.

Chu, K., J. Vojtchovsky, B. H. McMahon, R. M. Sweet, J. Berendzen, and I. Schlichting. 2000. Structure of a ligand-binding intermediate in wild-type carbonmonoxy myoglobin. *Nature.* 403:921–923.

Cordone, L., A. Cupane, M. Leone, and E. Vitrano. 1990. Thermal behavior of the 760-nm absorption band in photodissociated sperm whale carbonmonoxymyoglobin at cryogenic temperature: dependence on external medium. *Biopolymers.* 29:639–643.

Dickerson, R. E., and I. Geis. 1983. Hemoglobin: Structure, Function, Evolution, and Pathology. Benjamin/Cummings, Menlo Park, CA.

Eaton, W. A., and J. Hofrichter. 1981. Polarized absorption and linear dichroism spectroscopy of hemoglobin. *Methods Enzymol.* 76:175–261.

Elber, R., and M. Karplus. 1990. Enhanced sampling in molecular dynamics: use of the time-dependent Hartree approximation for a simulation of carbon monoxide diffusion through myoglobin. *J. Am. Chem. Soc.* 112:9161–9175.

Engler, N., A. Ostermann, A. Gassmann, D. C. Lamb, V. E. Prusakov, J. Schott, R. Schweitzer-Stenner, and F. G. Parak. 2000. Protein dynamics in an intermediate state of myoglobin: optical absorption, resonance Raman spectroscopy, and x-ray structure analysis. *Biophys. J.* 78:2081–2092.

Franzen, S., L. J. Moore, W. H. Woodruff, and S. G. Boxer. 1999. Stark-effect spectroscopy of the heme charge-transfer bands of deoxymyoglobin. *J. Phys. Chem. B.* 103:3070–3072.

Frauenfelder, H., S. G. Sligar, and P. G. Wolynes. 1991. The energy landscapes and motions of proteins. *Science.* 254:1598–1603.

Hartmann, H., S. Zinser, P. Komninos, R. T. Schneider, G. U. Nienhaus, and F. Parak. 1996. X-ray structure determination of a metastable state

of carbonmonoxy myoglobin after photodissociation. *Proc. Natl. Acad. Sci. U.S.A.* 93:7013–7016.

Hirota, S., T. Li, G. N. Phillips, J. S. Olson, M. Mukai, and T. Kitagawa. 1996. Perturbation of the $Fe-O_2$ bond by nearby residues in heme pocket: observation of ν_{Fe-O_2} Raman bands for oxymyoglobin mutants. *J. Am. Chem. Soc.* 118:7845–7846.

Huang, J., A. Ridsdale, J. Wang, and J. M. Friedman. 1997. Kinetic hole burning, hole filling, and conformational relaxation in heme proteins: direct evidence for the functional significance of a hierarchy of dynamical processes. *Biochemistry.* 36:14353–14365.

Iizuka, T., H. Yamamoto, M. Kotani, and T. Yonetani. 1974. Low temperature photodissociation of heme proteins: carbon monoxide complex of myoglobin and hemoglobin. *Biochim. Biophys. Acta.* 371:1715–1729.

Jackson, T. A., M. Lim, and P. A. Anfinrud. 1994. Complex nonexponential relaxation in myoglobin after photodissociation of MbCO: measurement and analysis from 2 ps to 56 μs. *Chem. Phys.* 180:131–140.

Johnson, J. B., D. C. Lamb, H. Frauenfelder, J. D. Müller, B. H. McMahon, G. U. Nienhaus, and R. D. Young. 1996. Ligand binding to heme proteins. VI. Interconversion of taxonomic substates in carbonmonoxy myoglobin. *Biophys. J.* 71:1563–1573.

Kneller, G. R., and J. C. Smith. 1994. Liquid-like side-chain dynamics in myoglobin. *J. Mol. Biol.* 242:181–185.

Kushkuley, B., and S. S. Stavrov. 1996. Theoretical study of the distal-side steric and electrostatic effects on the vibrational characteristics of the FeCO unit of the carbonylheme proteins and their models. *Biophys. J.* 70:1214–1229.

Lambright, D. G., S. Balasubramanian, and S. G. Boxer. 1991. Protein relaxation dynamics in human myoglobin. *Chem. Phys.* 158:249–260.

Li, T., M. L. Quillin, G. N. Phillips, and J. S. Olson. 1994. Structural determinants of the stretching frequency of CO bound to myoglobin. *Biochemistry.* 33:1433–1446.

Lim, M., T. A. Jackson, and P. A. Anfinrud. 1993. Nonexponential protein relaxation: dynamics of conformational change in myoglobin. *Proc. Natl. Acad. Sci. U.S.A.* 90:5801–5804.

Lim, M., T. A. Jackson, and P. A. Anfinrud. 1997. Ultrafast rotation and trapping of carbon monoxide dissociated from myoglobin. *Nature Struct. Biol.* 3:209–214.

McMahon, B. H., J. D. Müller, C. A. Wraight, and G. U. Nienhaus. 1998. Electron transfer and protein dynamics in the photosynthetic reaction center. *Biophys. J.* 74:2567–2587.

Mourant, J. R., D. P. Braunstein, K. Chu, H. Frauenfelder, G. U. Nienhaus, P. Ormos, and R. D. Young. 1993. Ligand binding to heme proteins. II. Transitions in the heme pocket of myoglobin. *Biophys. J.* 65:1496–1507.

Nienhaus, G. U., J. Heinzl, E. Huenges, and F. Parak. 1989. Protein crystal dynamics studied by time-resolved analysis of X-ray diffuse scattering. *Nature.* 338:665–666.

Nienhaus, G. U., J. R. Mourant, K. Chu, and H. Frauenfelder. 1994. Ligand binding to heme proteins. The effect of light on ligand binding in myoglobin. *Biochemistry.* 33:13413–13430.

Nienhaus, G. U., J. R. Mourant, and H. Frauenfelder. 1992. Spectroscopic evidence for conformational relaxation in myoglobin. *Proc. Natl. Acad. Sci. U.S.A.* 89:2902–2906.

Nienhaus, G. U., and R. D. Young. 1996. Protein dynamics. *In* Encyclopedia of Applied Physics, Vol. 15. G. L. Trigg, editor. VCH Publishers, New York. 163–184.

Oldfield, E., K. Guo, J. D. Augspurger, and C. E. Dykstra. 1991. A molecular model for the major conformational substates in heme proteins. *J. Am. Chem. Soc.* 113:7537–7541.

Olson, J. S., and G. N. Phillips. 1996. Kinetic pathways and barriers for ligand binding to myoglobin. *J. Biol. Chem.* 271:17593–17596.

Ostermann, A., R. Waschipky, F. G. Parak, and G. U. Nienhaus. 2000. Ligand binding and conformational motions in myoglobin. *Nature.* 404:205–208.

Phillips, G. N., M. L. Teodoro, T. Li, B. Smith, and J. S. Olson. 1999. Bound CO is a molecular probe of electrostatic potential in the distal pocket of myoglobin. *J. Phys. Chem. B.* 103:8817–8829.

Quillin, M. L., T. Li, J. S. Olson, G. N. Phillips, Y. Dou, M. Ikeda-Saito, R. Regan, M. Carlson, Q. H. Gibson, H. Li, and R. Elber. 1995. Structural and functional effects of apolar mutations of the distal valine in myoglobin. *J. Mol. Biol.* 245:416–436.

Sassaroli, M., and D. L. Rousseau. 1987. Time dependence of near-infrared spectra of photodissociated hemoglobin and myoglobin. *Biochemistry.* 26:3092–3098.

Schlichting, I., J. Berendzen, G. N. Phillips, and R. M. Sweet. 1994. Crystal structure of photolysed carbonmonoxy-myoglobin. *Nature.* 371: 808–812.

Springer, B. A., K. D. Egeberg, S. G. Sligar, R. J. Rohlfs, A. J. Mathews, and J. S. Olson. 1989. Discrimination between oxygen and carbon monoxide and inhibition of autooxidation by myoglobin. Site-directed mutagenesis of the distal histidine. *J. Biol. Chem.* 264:3057–3060.

Šrajer, V., and P. M. Champion. 1991. Investigations of optical line shapes and kinetic hole burning in myoglobin. *Biochemistry.* 30:7390–7402.

Šrajer, V., L. Reinisch, and P. M. Champion. 1988. Protein fluctuations, distributed coupling, and the binding of ligands to heme proteins. *J. Am. Chem. Soc.* 110:6656–6670.

Stavrov, S. S. 2001. Optical absorption band III of deoxyheme proteins as a probe of their structure and dynamics. *Chem. Phys.* 271:145–154.

Steinbach, P. J., A. Ansari, J. Berendzen, D. Braunstein, K. Chu, B. R. Cowen, D. Ehrenstein, H. Frauenfelder, J. B. Johnson, D. C. Lamb, S. Luck, J. R. Mourant, G. U. Nienhaus, P. Ormos, R. Philipp, A. Xie, and R. D. Young. 1991. Ligand binding to heme proteins: the connection between dynamics and function. *Biochemistry.* 30:3988–4001.

Stryer, L. 1995. Biochemistry, 4th ed. Freeman Publications, San Francisco.

Teng, T.-Y., V. Šrajer, and K. Moffat. 1994. Photolysis-induced structural changes in single crystals of carbonmonoxy myoglobin at 40 K. *Nature Struct. Biol.* 1:701–705.

Tilton, R. F., I. D. Kuntz, and G. A. Petsko. 1984. Cavities in proteins: structure of a metmyoglobin-xenon complex solved to 1.9 Å resolution. *Biochemistry.* 23:2849–2857.

Xie, X., and J. D. Simon. 1991. Protein conformational relaxation following photodissociation of CO from carbonmonoxymyoglobin: picosecond circular dichroism and absorption studies. *Biochemistry.* 30:3682–3692.